ELSEVIER

CFD-based analysis of pumped storage power plants implementing hydraulic short circuit operations

Alessandro Morabito *, Elena Vagnoni

Technology Platform for Hydraulic Machines, EPFL, Lausanne, Switzerland

ARTICLE INFO

ABSTRACT

Hydraulic short circuit (HSC), corresponding to the simultaneous operation of the pumps and turbines, enhances the power flexibility of a pumped storage power plant (PSPP). However, comprehensive analyses are imperative to guarantee a secure and reliable operation within this novel operational mode. Unforeseen engaging dynamics may perturb the safe operation of the groups. The existing literature still lacks comprehensive analysis concerning the water flow structures and turbomachine performances during HSC operations across the entire hydraulic circuit. This paper evaluates the fluid-dynamic interactions between the units during HSC operations using 3D unsteady-state CFD simulations of an existing PSPP not designed for enduring such conditions. The total pressure evolution in the upstream trifurcation and consequent effects on the turbine performance are discussed by the selected HSC configurations. In the trifurcation, between the pumping unit and the turbine, the relative head loss reaches 1,78% and, eventually, anomalies of the velocity field are documented on a case-by-case basis. Moreover, the pump operations are investigated in HSC operations with the matter of efficiency detriments, cavitation and air entrainment risk. The results highlight that the pumping unit in HSC compared to the baseline operation undergoes a reduction in hydraulic efficiency up to 0.51% due to the operation of adjacent turbine. The documented observations led to the application of additional criteria for the safe and stable governing control of the PSPP in HSC.

1. Introduction

In the past few decades, the deployment of pumped storage power plants (PSPP) has been instrumental in addressing the intermittent nature of renewable energy sources increasingly penetrating the majority of electric power systems [1]. Recent economic trends and policy dynamics have emphasized the need for enhanced flexibility in both power generation and storage modes. In PSPP, such operating control, which could be awarded by ancillary service retributions depending on the local energy market regulations, is partially achieved in generation mode with the power adjustment provided by the Francis turbine guide vanes or by the Pelton turbine injectors. However, in pumping mode, there is no possibility to manage the power consumption [2] because the discharge is mainly a result of the head as a boundary condition, and the guide vane regulation law, which is usually optimized for best efficiency operation [3]. Exceptionally, variable speed and seldom geometry regulations allow PSPP plants to extend their operating flexibility. However, when it comes to already existing pumped storage power plants (PSPP), the economic viability of incorporating variable speed capacity may be less favorable, particularly for smaller-scale

hydro projects [4]. Hydraulic short circuit (HSC) configuration, corresponding to the simultaneous operation of the pumps and turbines, enhances the power consumption flexibility of PSPP [5]. The main advantage of this practice is regulating the net absorbed energy by the PSPP with the power regulation range of the turbine operation [3]. Suppose the hydropower system is equipped with a ternary configuration (or with multiple reversible units); in that case, without incurring large investments, the HSC can be obtained and supply primary and secondary frequency regulation services to the transmission system operators (TSOs) within a larger marketable capacity [6].

The HSC principle is implemented in only a limited number of active applications worldwide. However, both academic [7] and industrial communities [8] have shown a growing enthusiasm for exploring the economic viability of this emerging operation. There is a keen interest in maximizing market participation and optimizing reserve schedule to ensure profitability in HSC operations [9]. Moreover, the pertinence of HSC operation for grid stability has been confirmed by several studies. Nicolet [10] has simulated an islanded power network in SIMSEN with a hydraulic plant equipped with either variable speed technology or a

---

ternary unit operating in HSC mode. Simulating disturbances in the network, they concluded that "both solutions contribute to power network stability by providing regulating power services". Perez-Diaz [11] also simulated an islanded power network, this time with Matlab-Simulink. They showed that HSC operation meets the requirements for primary, secondary, and tertiary load-frequency regulation. Chazarra [7] studied the economic viability of a ternary plant with and without HSC and concluded that the pay-back periods are reduced when using HSC operation.

The existing studies on HSC operation mainly concentrate on the simulation of the bi- or trifurcation, since in this operating condition, the water flows in directions the waterways were not designed for. This can lead to flow instabilities and increased head losses. Computational fluid dynamics (CFD) simulations are carried out to obtain more details of the water flow structures during HSC within the hydraulic circuit. Huber et al. [12] conducted CFD simulations to investigate the flow characteristics and head losses of a T-junction planned in the Kopswerk II under three different HSC operating conditions. An alternative T-junction was simulated to prove a better-computed design in flow properties and lower head losses. Decaix [13] simulated by CFD two bifurcations and one trifurcation of the complex Grand-Maison power plant operating in HSC concluding that the head losses in this section correspond to less than 1% of the gross head and that no flow instabilities are present in the bifurcations, but low-frequency oscillations of the total pressure are locally observed.

Despite the valuable insights provided by these studies, there remains a lack of in-depth analysis in the literature regarding the water flow structures during HSC within the entire hydraulic circuit. Currently, there are limited case studies available in the literature that examine upstream interconnections, and to the authors' knowledge, there are no reports on the interactions and operating perturbations downstream. This work provides an unique comprehensive research, addressing this gap by expanding the scope to include the impacts of HSC on turbomachine performances. Finally, this paper offers thoroughly detailed guidelines for the necessary CFD simulations to assess the feasibility of HSC, incorporating numerous components within the PSPP hydraulic circuit.

1.1. Contribution of the paper

Overall, the novelty of this paper concerning the extensive study of the HSC operations in the investigated PSPP can be summarized as follows:

- This paper evaluates the unexplored fluid-dynamic interaction between the units during HSC operations using unsteady-state CFD simulations, highlighting the technical clarifications to ensure the safe and stable operation of existing installations in this new mode of operation.
- The PSPP trifurcation in HSC is subject to different pressure loss patterns and fluctuations. The investigation of flow development from this perspective is unprecedented, particularly regarding its role as a potential cause of performance interference at the turbine inlet during HSC operations.
- The numerical results illustrate the engaging dynamics in the downstream reservoir to exclude or quantify the development of vortical structures which may perturb the operation of the groups. In the literature, this particular area has yet to receive extensive investigation.
- The paper methodology and results contribute to the understanding of the HSC operations and their impacts on the investigated PSPP performance. It provides unique insights into the challenges faced by the system and offers recommendations for improvement. These contributions can inform future research and policy decisions to enhance the effectiveness of HSC.

1.2. Paper structure

This paper presents the implemented methodology for the CFD simulations in Section 2. Here, the involved geometries are described, and the following subsections elaborate on the adopted numerical method, and the boundary conditions for the trifurcation and downstream domains. The results of the analysis of the trifurcation and the downstream are validated and shown in Section 3, whereas the modifications of the PSPP controlling system for safe HSC operations are discussed in Section 4. Finally, the conclusions are drawn in Section 5.

2. Methodology

This research studies the quantification of HSC potential for an existing PSPP that was commissioned in the early 1970s. This hydropower plant includes three equal Francis pump-turbines. Concerning power management and dispatching strategy, three operations are finally available in the PSPP case: generating mode, pumping mode and HSC, as described in Fig. 1 under the variation of flow rate, head and power. Generating mode profits of operational control of the guide vanes to modulate the discharge and thus the power production. Three areas are defined at positive power (generation): one for a single turbine activated and for two or three groups running in parallel. Then, three characteristic curves at negative power (consumption) and negative discharge (towards the upper reservoir) define the pumping mode. Finally, the admissible operating ranges in HSC are obtained by translating the generating surfaces by the pumping characteristic.

As the system involves a trifurcation with reversible pump-turbines at the end of each branch, various configurations for potential HSC operation must be studied. The case study will be referred by acronyms where *P* refers to a pumping unit, *O* closed branch, and *T* refers to a turbine branch, with the order of the acronyms referencing the order of units 1 to 3. The studied cases include HSC operations with one or two units in pump mode, i.e. POT, PTO, OPT, PTP, and PPT. Due to the geometrical symmetries between group 1 and 3, the TOP, OTP, TPO, and TPP cases can be regarded as being in similarity with the equivalent cases mentioned earlier.

While steady-state simulations provide preliminary outlooks of the pressure losses and velocity field [14], Unsteady-RANS simulations are carried out for the five cases for two HSC operating limits. Those conditions are defined in relation to the net power consumption of the whole PSPP, as follows:

- HSC at maximum consumed power: $MAX(P_{pump}(H) - P_{turbine}(H, \alpha))$
- HSC at minimum consumed power: $MIN(P_{pump}(H) - P_{turbine}(H, \alpha))$

where H is the available head at the unit and α is the turbine guide vane opening angle (GVO). At HSC - $Pmax$ condition a fraction of the pump discharge is engaged by the turbine in part load. At HSC - $Pmin$, the unit in turbine mode is generating at its maximum dropping the PSPP power net consumption at its minimum. To succeed, the upper reservoir is also feeding the turbine.

2.1. Geometry description

The PSPP under investigation is equipped with three equal Francis-type reversible pump-turbines of 71.8 MW power supply capacity each, connected by a single 800-meter-long penstock. The specific speed of the nine-blade reversible Francis-type impeller is 112.2 (metric), running at a fixed speed of 375 rpm. The simulated research domain is divided into the waterway trifurcation of the PSPP and the pump-turbine units connected by the lower reservoir. A 3D scan on site has obtained the geometry of the trifurcation internal surfaces. The penstock diameter coming from the upper reservoir is 5.6 m large and it splits into three branches, the diameter of which converges from 2.7 to 2 meters when reaches the inlet of the pump-turbine spiral casing. The
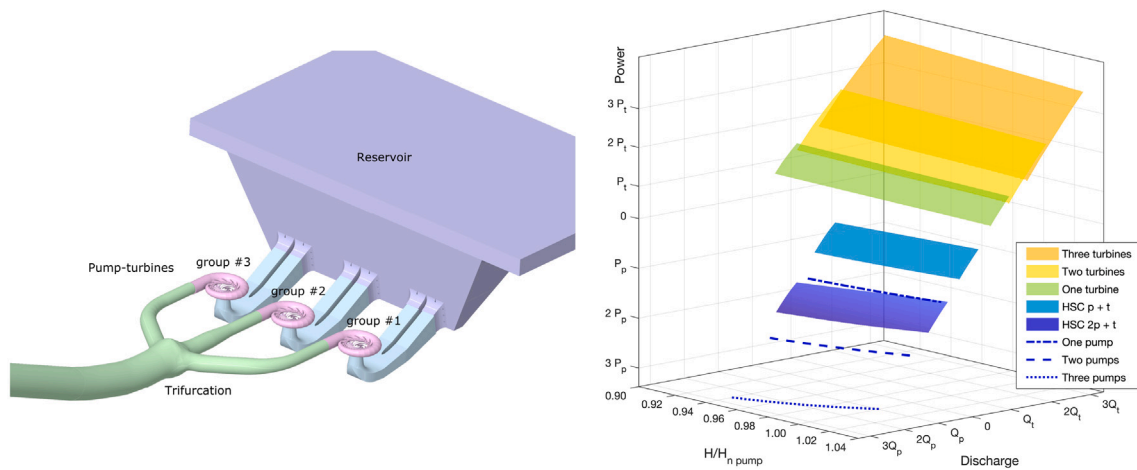
Fig. 1. Overview of the investigated PSPP and power regulation chart.

Table 1
Mesh sizes and quality reports.

Element	Body size target and growth rate	Boundary layers	First cell size and growth rate	Minimum Orthogonality	Maximum Aspect Ratio
Runner	10/25 mm, 1.20	8	0.2 mm, 1.4	0.35	200
Draft-tube	30/50 mm, 1.05	8	8 mm, 1.2	0.5	13
Vanes 11.5°	25 mm, 1.20	6	0.2 mm, 1.5	0.3	300
Vanes 22.5°	25 mm, 1.20	6	0.2 mm, 1.5	0.34	280
Casing	70 mm, 1.20	6	0.5 mm, 1.5	0.4	300
Reservoir	70 mm, 1.05	8	8 mm, 1.2	0.26	220
Reservoir, top	300 mm, 1.05	–	–	0.5	8
Reservoir, grid	15 mm, 1.20	5	4 mm, 1.2	0.8	140

two branches on the side bend of 50° with 8 meters of inner radius curvature, and they align with the pump-turbine in the middle (unit 2). At the intersection, two stiffeners up to 0.6 m tall surround the connection with the central branch.

The downstream domain includes the units involved in the specific HSC operation, the reservoir, and the nearby river. The three units' axes are 14 m apart, and the edges of the draft tube intakes are distant by 6.5 m. The reservoir is shaped as a trapezoidal pyramid 21-meter-deep and the pump-turbine intakes are 2.2 m from the front wall, which goes up towards the river with a 60° slope. In addition, the trash racks at the intakes are reproduced in the domain. The geometry of the lower reservoir plays a key role in the interaction of the units during HSC operations. If units in opposite modes are too close the normal performances could be depleted, and efficiency detriment could occur.

2.2. Mesh analysis

Polyhedral meshes are generated for discretizing the computational fluid domain with the ANSYS (v22R) fluent software. Finer local sizing is implemented in the proximity of critical areas as in the nearabout of the stiffeners. In addition, an inflation mesh technique is used for the fluid volume near the pipe wall in agreement with the y+ required by the turbulence model. A grid independency study is carried out to monitor the variation of the averaged pressure in control sections for converged solutions by the increasing number of grid nodes. The plots in Fig. 2 show the total pressure losses in the trifurcation in pumping and with three units in turbine mode versus the mesh size. The selected trifurcation mesh has an average cell size of 238.6 mm and an overall number of elements of 3.7 million. It involves 5 inflation layers starting at a height of 1 mm and with a growth rate of 1.5, aiming for a y+ between 50 and 200. The downstream domain elements are examined in a sensitivity test locally. The runner, stay vanes and guide vanes, and volute are also generated with a polyhedral unstructured grid coupled with a structured boundary layer: the results of the tests are shown in

the plots on the right of Fig. 2. Marginal differences are noted in quality measures for vanes at various opening angles; the acceptance criteria are always reached for all the GVOs. Hence, spiral casing, vanes and draft tube are tested according to the total pressure losses relative to the selected mesh. The analysis of the reservoir mesh deals with the criteria of preserving the main characteristics of the contiguous draft tubes in the bottom part of the reservoir and facing the disturbance of the trash rack at each intake. The following Table 1 summarizes the main characteristics of the selected meshes.

2.3. Numerical method

Single-phase simulations are performed by the CFD software Ansys Fluent 2022R1 with the realizable k–ϵ, and SST k–ω turbulence models respectively for the trifurcation and downstream domains. The y+ values are consistent with the model adopted for all the simulated discharge ranges. The SIMPLEC and COUPLED schemes are chosen to deal with the pressure–velocity coupling and a second-order upwind spatial discretization scheme is employed. Under-relaxation is activated than enough for the pressure and turbulence factors. The convergence criterion is not defined unequivocally by examining the residuals, but also by minimal imbalance of mass (<0.01% of total mass) and stable outputs per time-step. To comply with convergence criteria per time-step (<10^{-5}) and repeatability, a maximum of 100 iterations are set sufficient in both the trifurcation and in the downstream research domains. A comprehensive table on the CFD setup is given in Table 2.

2.4. Set-up of the trifurcation analysis

The domain consists of the three branches and waterways portion of 25 meters towards the upper reservoir. Moreover, extensions of ten times the diameter are conveniently added to the outlets to ease the numerical computations. In the trifurcation set of simulations, the inlet boundary is velocity inlet time-dependent extracted from the
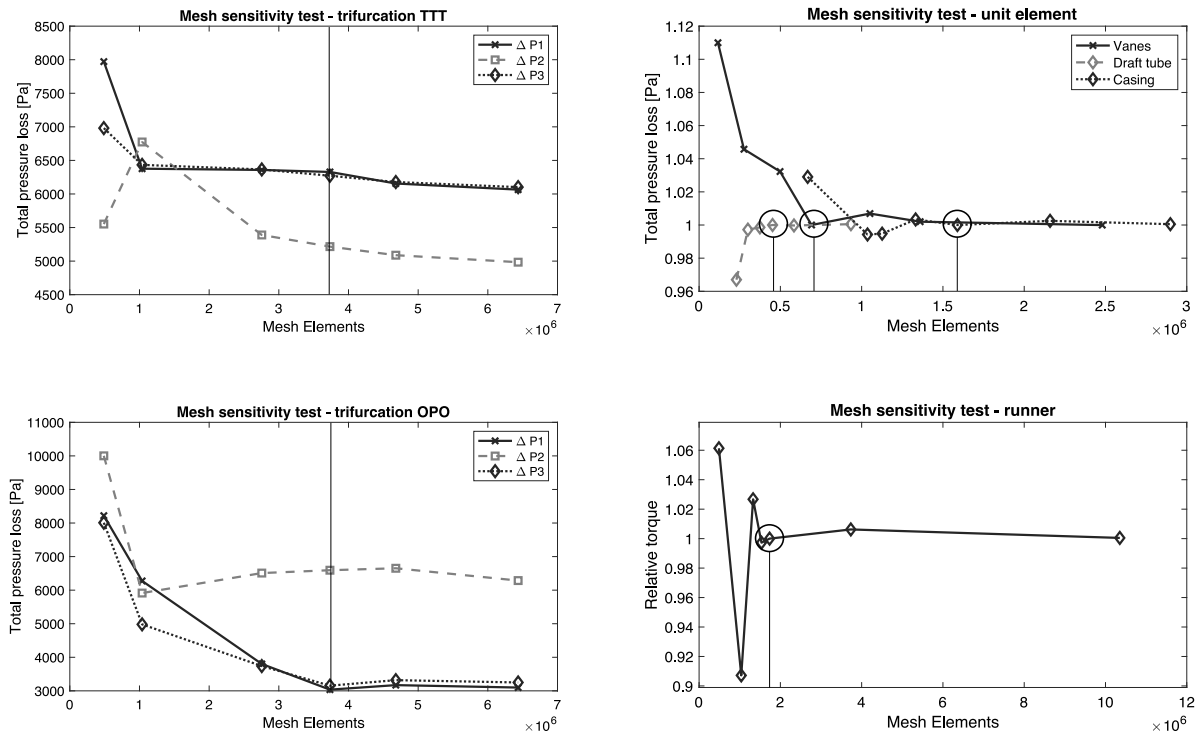
Fig. 2. Mesh sensitivity test for investigated domains. Vertical lines mark the selected size of the meshes. The extensions are not taken into account in the mesh size counting.

Table 2
Simulations setup.

Gravitational acceleration	9.81 m/s^2
Water viscosity	0.001003 kg/(m s)
Water density	998.2 kg/m^3
Reference pressure	0 Pa
coordinates	(0, −12 m, 17.73 m)
Solver	Type: Pressure based
	pump-turbine period: 0.16 s
	4.4444 10^{-6} s ≤ time-step ≤ 1.3333 10^{-4} s
	Time: Steady or Transient
Turbulence models	Trifurcation: realizable k–ϵ, Enhanced wall treatments
	Downstream: SST k–ω, Enhanced wall treatments
Walls	No-slip condition
	pump mode: 375 rev/min
	turbine mode: −375 rev/min
Rotation axis	unit 1: (−14 m, 0, 0), (0,0,1)
	unit 2: (0, 0, 0), (0,0,1)
Solution methods	Scheme: SIMPLEC or Coupled
	Gradient: Least Squares Cell-based
	Pressure: Second Order
	Momentum, TKE, TDR : Second Order Upwind

3D simulation of the pump. In contrast, the outlet boundaries to the upper reservoir and turbine are set as mass flow outlet and pressure outlet respectively. The inlet velocity profiles replicate the velocity components exiting the spiral casing of the unit in pump mode. Such a velocity pattern changes in time and its role in the trifurcation simulation is proven to be relevant in the description of the velocity field [14]. The investigated operations can be summarized in Table 3 where head, discharge, and power are normalized by the nominal values per operation modes (H_n, Q_n, P_n). The divergence between the pressure inlet (from the pump) and pressure outlet (at the turbine inlet) is given by the estimated pressure losses in the trifurcation by preliminary RANS simulations. The estimated available head at the outlet provides the basis for defining the operating point of the turbine. Transient simulations are performed for a total of ≥ 20 s. In this time

lap, a fully developed velocity profile is recorded at the outlet of the domain for all the configurations.

2.5. Set-up of the downstream analysis

In normal turbine operation, the flow exiting the draft tube hits the front wall and rises at high speed along the inclined wall. Recirculation is foreseen between the bottom reservoir and the surface in relation to the depth of the river. The higher the water level, the slower the recirculation. Eventually, the explored domain includes the units and the reservoir at the minimum water level (Z_{LIM}) of the downstream basin, where low hydrostatic pressure occurs, and more likely air entrainment may happen at the pump suction side (Fig. 3).

External conditions might perturb the flow patterns at turbine outlets or pumping intakes in the reservoir (e.g. river's current), but any specific condition is predictable in the actual analysis. Therefore, all the sources of perturbation independent of the PSPP apparatus are placed far from the unit. To this matter, additional inlet and outlet boundaries are defined at the river sides to comply with the balance of mass. These openings also prevent the possibility of relying solely on the discharge from the turbine to feed the pump's suction, compelling the solver to simulate an artificial scenario.

The PTO and TPO configurations are examined to evaluate the impact of the proximity of the reservoir's side wall to the unit, both in pumping mode and generating mode, and whether the distance between the groups is sufficient to guarantee proper functioning. The investigated operations can be summarized in Table 4.

2.6. Methodological constraints and considerations

In the defined methodology, three main limitations are encountered, necessitating thoughtful mitigation. Firstly, it is acknowledged that only two case studies are described, representing the minimum and maximum power consumption of the PSPP. However, it is important to note that these two cases represent the most extreme operating conditions, allowing us to draw meaningful insights despite the limited

Table 3
Explored HSC operations conducted for the five configurations within the trifurcation domain.

Case name	HSC Power	Q_t/Q_p	Q_t/Q_p	Pump			Turbine		
	consumption $P/P_{n,p}$	1 pump	2 pumps	$H/H_{n,p}$	$Q/Q_{n,p}$	$P/P_{n,p}$	$H/H_{n,t}$	$Q/Q_{n,t}$	$P/P_{n,t}$
Pmax	0.66	0.5433	0.2716	0.96	1.09	1.06	0.96	0.53	0.42
Pmin	0.02	1.2473	0.6236	1.05	0.86	0.94	1.05	0.94	0.97
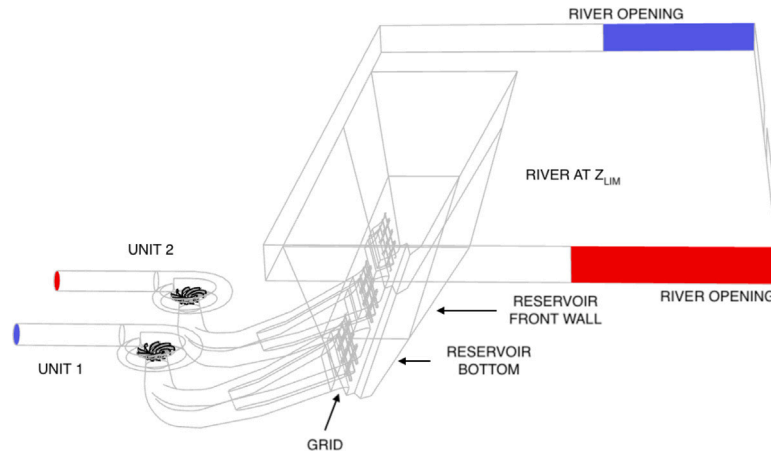
Fig. 3. Downstream domain including two units, the reservoir and water basin.

Table 4
Explored HSC operations conducted for PTO and TPO configurations within the downstream domains.

Case name	HSC Power	Q_t/Q_p	Pump			Turbine		
	consumption $P/P_{n,p}$	1 pump	$H/H_{n,p}$	$Q/Q_{n,p}$	$P/P_{n,p}$	$H/H_{n,t}$	$Q/Q_{n,t}$	$P/P_{n,t}$
Pmax	0.635	0.5616	0.98	1.06	1.04	0.977	0.52	0.43
Pmin	0.121	1.106	0.98	1.06	1.04	0.978	1.03	0.98

scope. Subsequently, the methodology assumes a perfect mirroring within the domain between units 1 and 3. Nonetheless, it is recognized that some flow patterns may not adhere strictly to this symmetry. It is anticipated that any deviations from perfect symmetry are likely to be minimal and therefore have negligible impact on the final findings. Lastly, limitations associated with CFD discretization approximations and algorithms are acknowledged. Turbulent flow, for instance, is complex and often requires specialized turbulence models to simulate accurately. Choosing an appropriate turbulence model for a specific flow regime can be challenging, and these models may have intrinsic limitations in certain scenarios (model accuracy, wall-bounded flow assumptions, anisotropy and rotating flows [15]). To address this, comprehensive model and mesh tests are conducted, aiming to mitigate potential errors in discretization and algorithmic approximations. Additionally, validations are crucial and extensively discussed to identify and address any unacknowledged errors in our CFD simulations. These measures are essential in ensuring the reliability and robustness of the presented methodology despite these inherent limitations.

3. Results

3.1. 3D simulation model validations

The implementation of the CFD analysis in the trifurcation is validated against experimental data retrieved during a fingerprint test on-site. Based on the recorded turbine GVO and power balance, the unit discharge can be indirectly retrieved by scaling the characteristic of the model to the prototype dimension. Unit speed ($n11$) and unit discharge ($Q11$) relate the similarity between the downsized model and prototype and are defined as follows:

$$Q_{11} = \frac{Q}{D^2 H^{0.5}} \qquad n_{11} = \frac{nD}{H^{0.5}} \tag{1}$$

With the estimated discharge in Eq. (1), it is possible to assess the pressure losses by the trifurcation. The numerical model is validated thanks to the reservoir water levels and local pressure measurements before and after the unit.

Moreover, the full-scale CFD turbomachine performances are found in agreement with the reduced scale model report provided by the manufacturer. Fig. 4 shows the URANS CFD simulated full-scale unit in turbine mode at several operations defined by two sets of points:

- Set-1: different GVO at the nominal discharge Q_n (red markers).
- Set-2: CFD results at fixed GVO (26.1°) and variable discharge (yellow markers).

The hydrodynamic performances of the Francis turbine are calculated from the head, discharge and computed torque on the runner walls. The operating points are graphed in unit speed ($n11$) and unit discharge ($Q11$) on the model test's hill chart, and the validation is assessed by comparing the efficiency and the GVO. The simulations of the reproduced runner globally agree with the model test in turbine mode. The efficiency is higher in the simulated full-scale geometry, and the best efficiency point is found to be closely aligned with the location indicated by the model test. Moreover, the Set-2 well replicate the trend of the fixed GVO despite a reasonable discrepancy of about 0.2°.

The performance transposition from the model to the prototype is subject to the methodology provided by IEC code no. 60193 [16]. In this case, a reference Reynolds number of $7 \cdot 10^6$ is considered to minimize the deviation

$$(\Delta\eta_h)_{pty \to md} = \delta_{ref} \left[\left(\frac{Re_{ref}}{Re_{pty}} \right)^{0.16} - \left(\frac{Re_{ref}}{Re_{md}} \right)^{0.16} \right] \tag{2}$$

where $\delta_{ref} = (1 - \eta_{h,\,pty,\,opt}) / \left[\left(\frac{Re_{ref}}{Re_{pty,\,opt}} \right)^{0.16} + \frac{1 - V_{ref}}{V_{ref}} \right]$ with V_{ref} equal to 0.7 for operation as turbine and 0.6 for operation as pump.
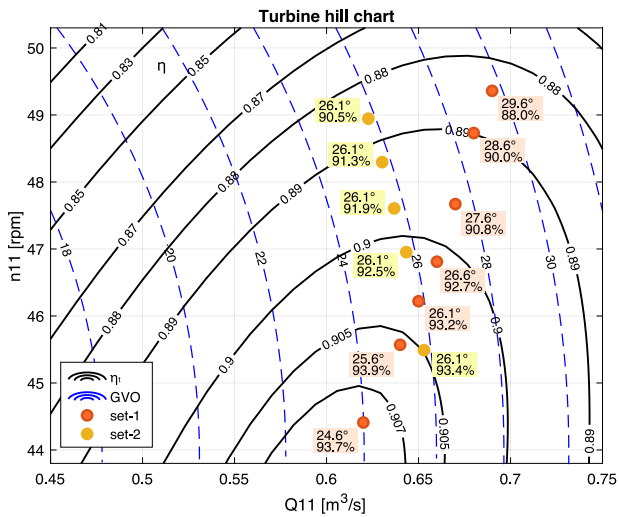
Fig. 4. Validation of two sets of CFD simulations over the model's turbine hill-chart. Each mark of the CFD simulation set is featuring GVO [°] and hydraulic efficiency for comparison to the manufacturer turbine hill-chart.
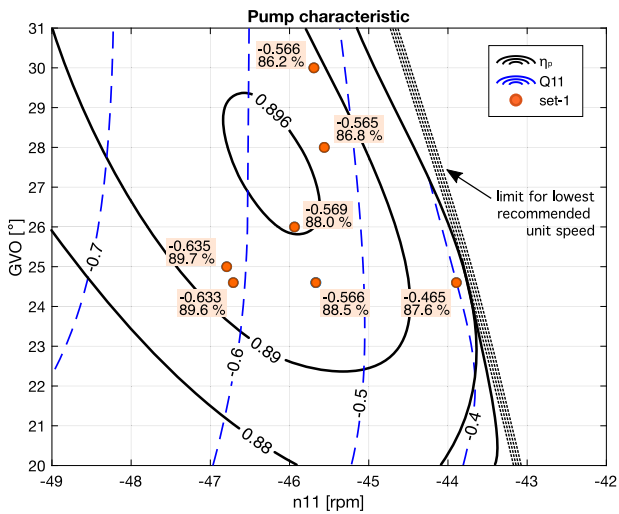

Fig. 5. Validation of the pump characteristic overlapping with CFD validation tests. Each mark of the CFD simulation set is featuring $Q11$ [m³/s] and hydraulic efficiency for comparison to the manufacturer pump characteristics.

The values of $\Delta\eta_{h,\ pty\to md}$ thins the difference between the model and CFD results at the best efficiency point from 2,2% to 1.4%.

In pump mode, the simulations' boundary conditions set the GVO and the discharge. The results deliver $n11$, $Q11$, and efficiency. Because of the favorable likeness of the discharge unit and efficiency with the model test (Fig. 5), it can be deduced that the numerical simulations align with the actual data from the site, thereby enhancing confidence in the prediction model. This validation process establishes a higher level of trust in the model's accuracy. Furthermore, the CFD methodology employed can be extended for future investigations. The Appendix of this paper contains a comprehensive compilation of the results.

3.2. PSPP trifurcation in HSC

The HSC operating mode induces alterations in the flow routes within the penstocks and the three branches when compared to the typical turbine or pump modes. Fractions of the pumped flow are redirected accordingly to the turbine and the upper reservoir. It is also conceivable that both the pump and upper reservoir jointly contribute to supplying discharge to the turbine. The effects of the vortices in the
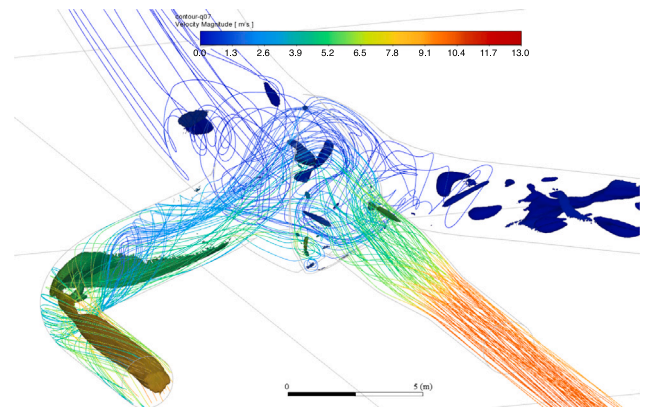

Fig. 6. Instantaneous view of the PTO $Pmin$ velocity streamlines and normalized 0.7 $Qcriterion$ iso-surface.
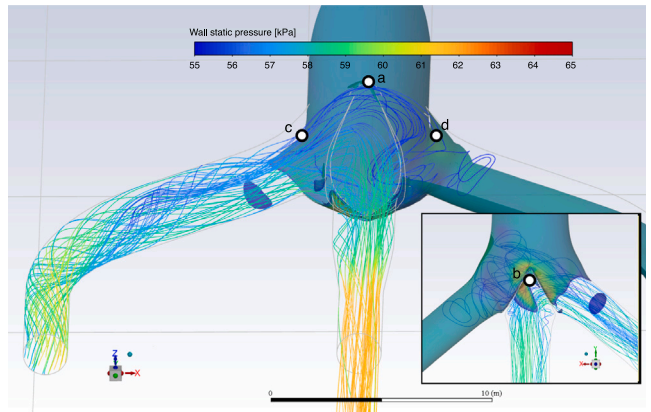

Fig. 7. Instantaneous view of the PTO $Pmin$ pressure at the wall clipped at $z = 0$ and detail of the pressure wall contour in the x–y plane.

pressure loss coefficient can individually be evaluated with an analysis of their formation, propagation and dissipation in the flow. Streamlines highlight flow deflections within the trifurcation and at the intersecting area and mixing zones. The instantaneous flow streamlines colored by velocity magnitude show the relevant flow vorticity and turbulence areas. In this section, only the PTO $Pmin$ case is shown. Fig. 6 provides the PTO - $Pmin$ case view of the streamlines and 0.7 normalized $Qcriterion$ iso-surface. The initial flow pre-rotation results from the pump-delivered velocity profile. Secondary flows leave faster streamlines and a larger vortex structure at external radii of the curvature towards the trifurcation centre. Indeed, the $Qcriterion$ iso-surface aims to depict the structure of the vortexes: it represents the local balance of the strain rate and magnitude of vorticity, defining vortices as regions where the magnitude of the vorticity is greater than the magnitude of deformation. The intensity given by the velocity contour on the iso-surface supports the interpretation of the vortex movement speed in the trifurcation. Once the flow reaches the broad intersecting area, the flow velocity drops. The flow coming from the pump inevitably hits the front wall of the trifurcation but in the $Pmin$ operating point, the turbine exploits discharge coming from the upper reservoir as well; this contribution helps the flow to turn in the turbine branch without scattering the streamlines in all directions. Then, the converging duct accelerates the flow towards the turbine with a residual swirl. Moreover, the lateral stiffeners contribute to generating small vortexes, focal points of local static pressure drop. However, the minimum pressure value metered in those areas is 6.9 kPa less than the area averaged value at the domain exit, namely the inlet to the turbine spiral casing. Overall, because the pump delivers a high head, the pressure values are sufficiently significant to prevent cavitation within the trifurcation.
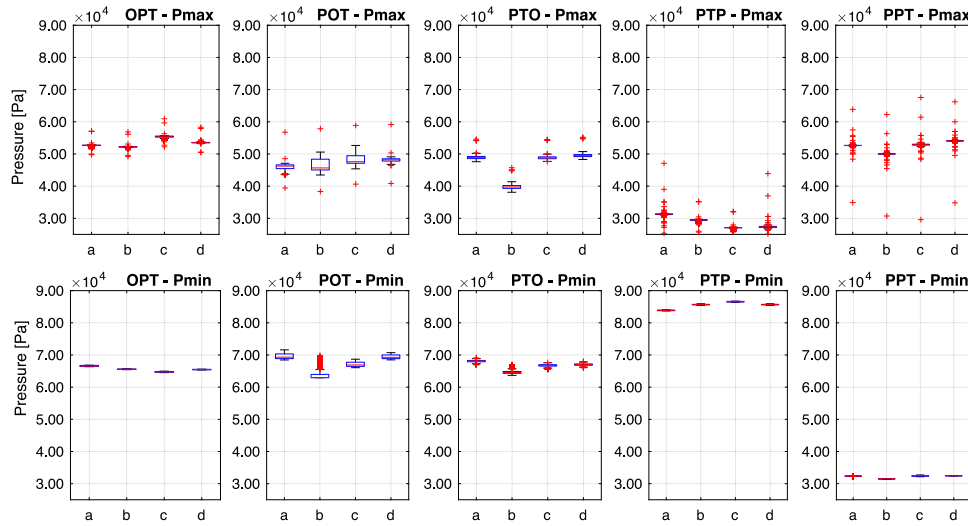
Fig. 8. Boxplots of pressure variation at four probes for the HSC operations.
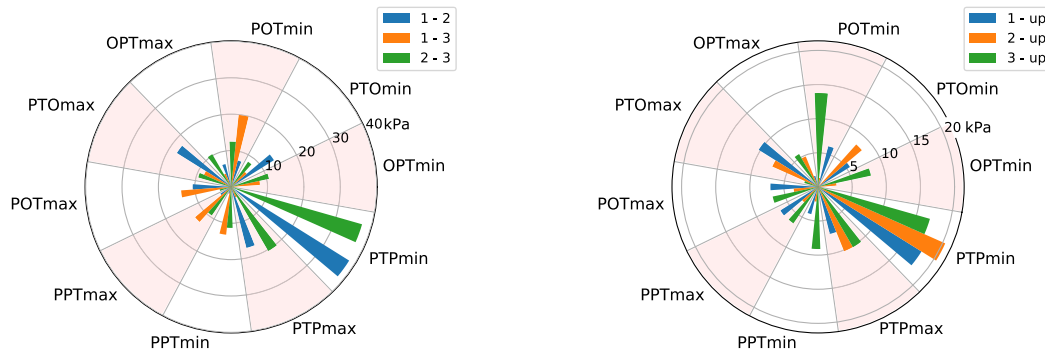

Fig. 9. Radar charts of the trifurcation pressure losses in kPa. The pressure drops are reported under the HSC operations and segments: (on the left) between the units (1–2, 1–3, and 2–3), and (on the right) towards the upper reservoir.

The static pressure contour on the walls illustrates concentrated areas of flow impact within the trifurcation (Fig. 7). The recorded wall stress is to add to the outlet pressure as the boundary condition at the turbine inlet is set with a zero pressure gauge. The mentioned figures refer to the latest converged time-step and a time-dependent analysis showed no relevant impulse on the wall: four probes on intersection walls (ⓐ, ⓑ, ⓒ, ⓓ) show limited oscillation bounded in 10 s as reported in the plots of Fig. 8. On each box, the central mark indicates the median, and the bottom and top edges of the box indicate the 25th and 75th percentiles, respectively. The whiskers extend to the most extreme data points not considered outliers, and the outliers are plotted individually using the red marker.

Since HSC operations were not initially foreseen during the PSPP's construction, it becomes crucial to quantitatively evaluate the head losses occurring at trifurcation per each possible configuration. The pressure losses obtained in a non-steady state are summarized in Fig. 9. The pressure gap between the units globally lies below 20 kPa, but the worst scenario is met with PTP - *Pmin* operation for 39 kPa of head loss between pump and turbine. Graphical representations of the pressure variation in trifurcation under the different HSC operations for the HSC cases are shown in Figs. 10–14. The pressure field, denoted as p_n, represents the total pressure normalized by the mass average value at the inlet section. The highest value is observed at the inlet that exhibits a non-uniform total pressure field. Gradually, p_n decreases due to losses in the pumping branch, reaching different pressures at the trifurcation

crossing section and within the main penstock, depending on whether the flow is coming from the first (curved) branch or the second (short and straight) branch. The entry point into the turbine branch varies depending on the HSC operation. Velocity magnitude and 2D streamlines, which depict the shear stress vector, are displayed in sections A and B of the turbine branch. Section A illustrates the exiting velocity profiles that, nevertheless, achieve a more axis-symmetrical distribution at the trifurcation outlet for most of the HSC configurations.

3.3. Interaction of the trifurcation in HSC and unit turbine

The extraction of the profiles at the trifurcation exit allows assessing the flow-field adaptation at the turbine inlet. The turbine operations involved in the second or third branch are characterized by a velocity vector field quasi-orthogonal to the turbine inlet section (≈ 90°). A series of plots in Fig. 15 illustrates the comparisons of the velocity angle in the trifurcation exit between the normal turbine operation (in red) and HSC operations (in black) marked with its standard deviation for 500 time-steps. The majority of the comparisons exhibit no notable disparities, but the operations in PTP - *Pmin*, PTO - *Pmax*, and POT - *Pmax* display the most affected with a deviation from the axial branch direction between 2 and 8 degrees.

A set of simulations is performed to assess the effects of the modified flow profiles coming from the trifurcation under HSC operations on the turbine's performance. Thus, the analysis concerns the PTP, POT and
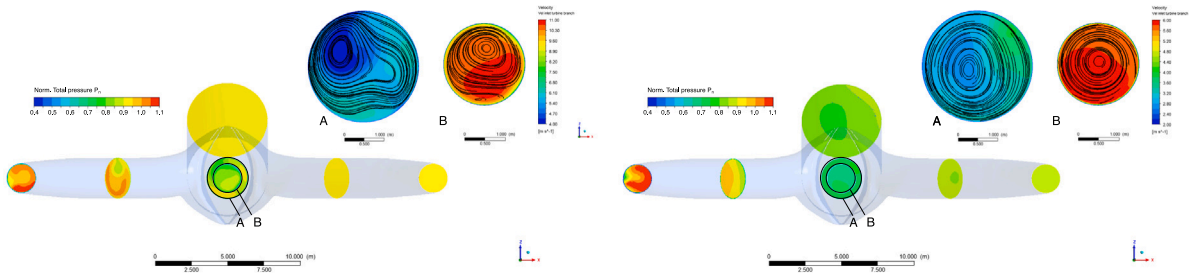
Fig. 10. PTO operations: total normalized pressure p_n and velocity 2D streamlines in two turbine branch sections.
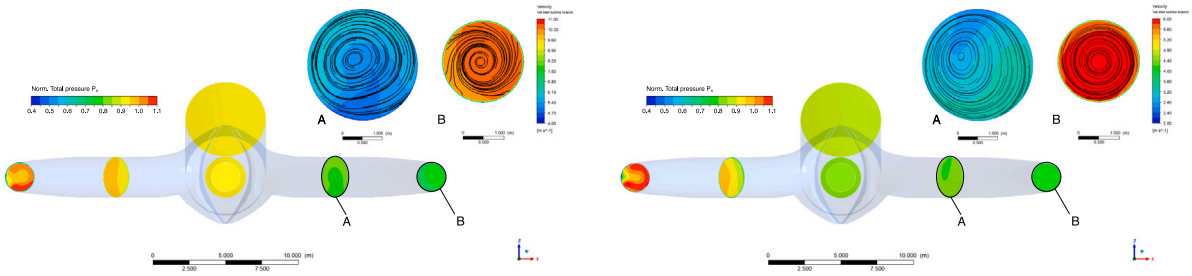

Fig. 11. POT operations: total normalized pressure p_n and velocity 2D streamlines in two turbine branch sections.
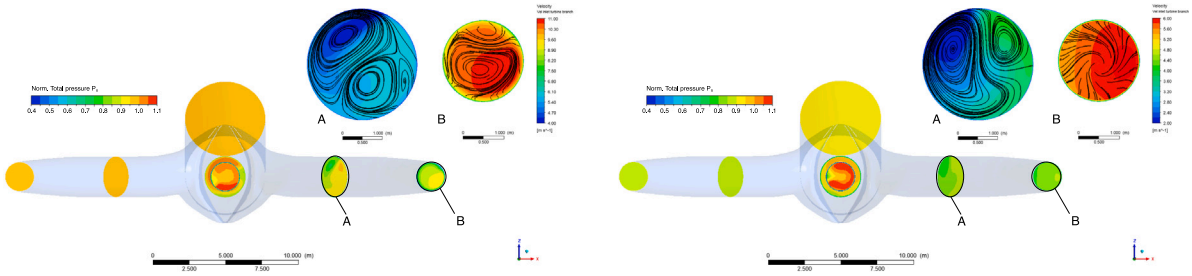

Fig. 12. OPT operations: total normalized pressure p_n and velocity 2D streamlines in two turbine branch sections.
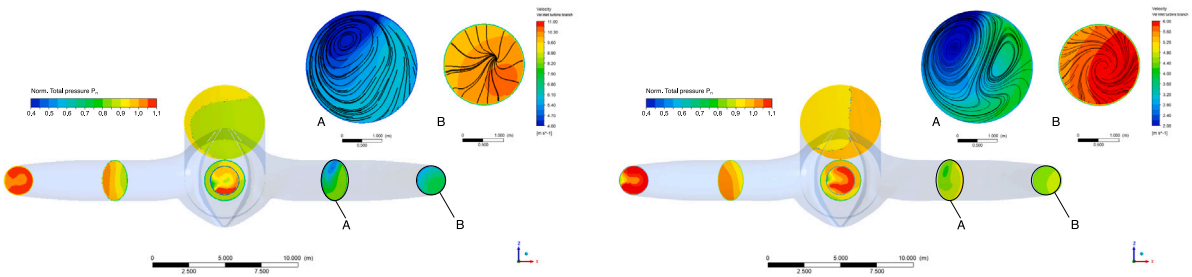

Fig. 13. PPT operations: total normalized pressure p_n and velocity 2D streamlines in two turbine branch sections.
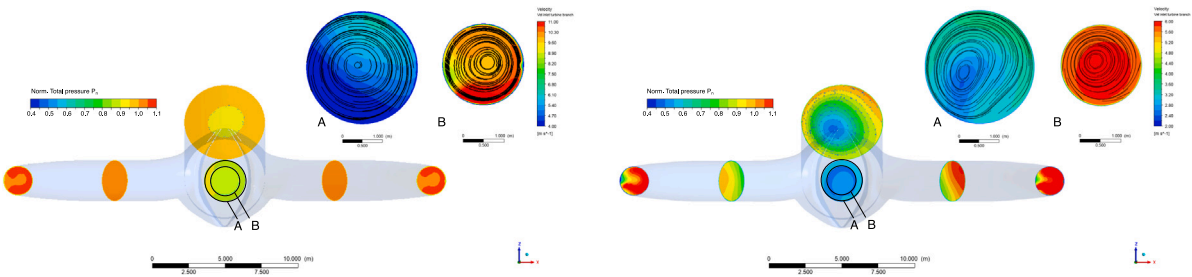

Fig. 14. PTP operations: total normalized pressure p_n and velocity 2D streamlines in two turbine branch sections.
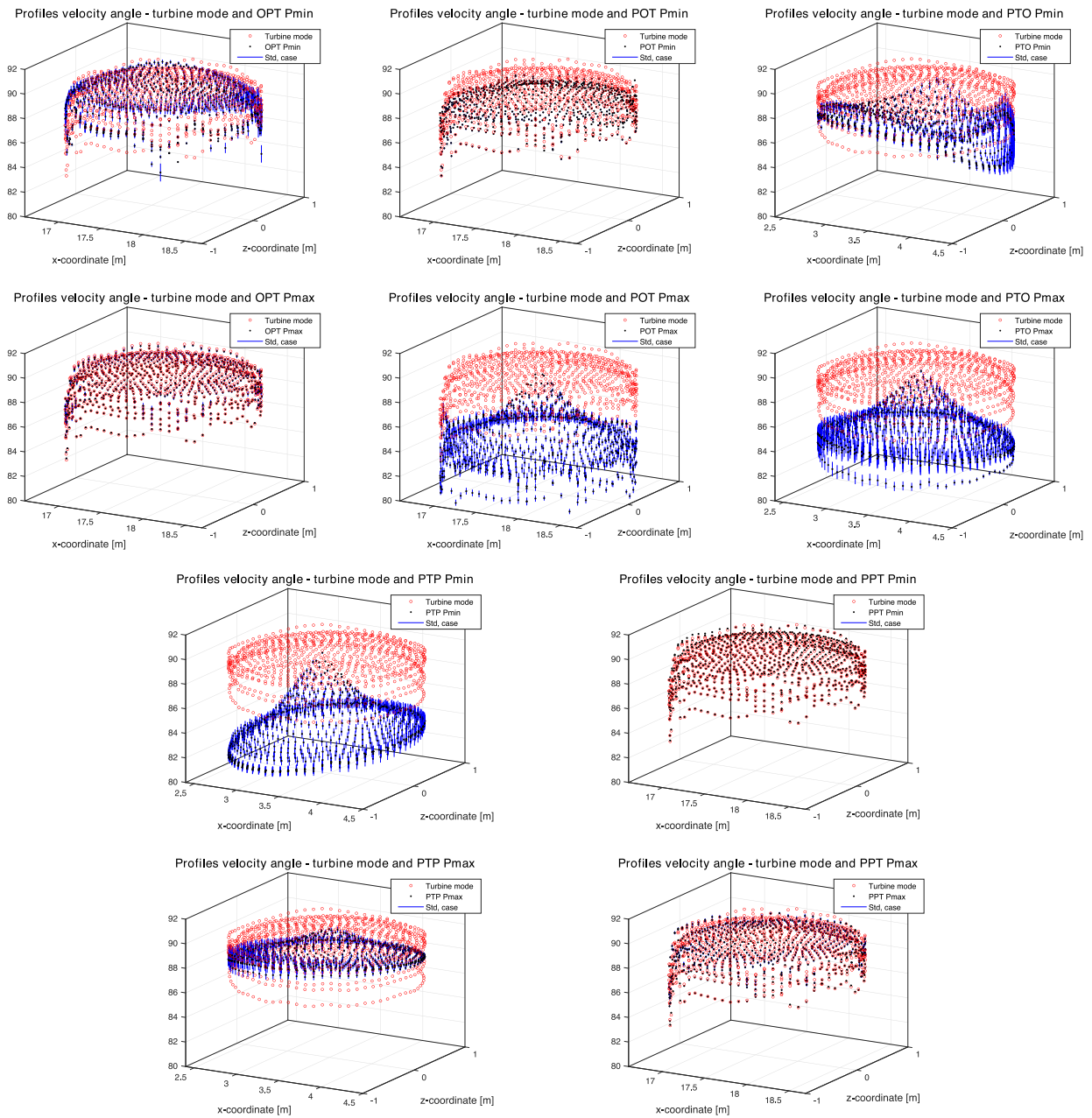
Fig. 15. Velocity angle comparison [deg] of the velocity profile entering the spiral casing between normal turbine and HSC.

PTO cases, in which larger deviations of the velocity field and relative pressure losses in the casing $\Delta H / H_{n,t}$ are reported (see Table 5). These results are compared to the undisturbed profiles for full-load and part-load turbine operation. For the undisturbed cases, which will be used as baseline, a mass flow inlet boundary condition normal to the section passage was used to obtain a uniform velocity profile. The discharge is set to $Q = 0.52Q_n$ and $Q = 0.94Q_n$ respectively for the *Pmax* operations and *Pmin* operations. The baseline mass flow inlet does not have any tangential or radial components. The average velocity magnitude is 5.77 m/s in part load case and 10.99 m/s in full load.

3.4. PSPP downstream analysis in HSC

The downstream cases are undertaken by identical boundary conditions (Table 4), only the location of the pump and turbine is inverted. It follows that, alternately, the pump and the turbine interact with an immediately smaller volume of the reservoir because of its adjacent vertical wall. Indeed, unit 1 is obstructed at its right limiting the free development of the flow. On the other hand, unit 2 benefits from a less constrained volume in front of the draft tube (Fig. 3). Each configuration is then simulated at different turbine performances, namely full load (HSC - *Pmin*) and deep-partial load (HSC - *Pmax*). Besides diverse turbine discharge rates, the turbine velocity profiles exiting the draft tube are distinct. Fig. 16 illustrates the instantaneous contours of the velocity in the normal component at the draft-tube exit. At full load ($Q = 1.03Q_n$), the discharge is released in the reservoir with an equally split distribution within the two passages of the draft tube. The profile illustrates a mirrored pattern with high velocity next to the external walls and a limited portion in back-flow at low speed. At part-load operation ($Q = 0.52Q_n$), the water flow engages a single draft-tube channel (section B) due to a vigorous residual swirl exiting the turbine. In the other channel (section A), a back-flow is reported in the draft-tube outlet. The velocity field in this section is under modest time-varying fluctuation within 10% of the time-averaged value.

Table 5

Comparison of turbine performance between undisturbed inlet flow (*Pmin* and *Pmax*) and HSC-perturbed flow.

	Pmin	*PTP − Pmin*	*Pmax*	*POT − Pmax*	*PTO − Pmax*
$Q_{in}/Q_{n,t}$	0.94	0.94	0.52	0.52	0.52
$\Delta H/H_{n,t}$, ‰	33.48	35.22	25.22	26.96	27.39
Torque, E+05 N m	16.5	16.4	9.50	9.47	9.44
$P/P_{n,t}$	0.903	0.899	0.520	0.513	0.516
Efficiency, %	92.27	92.05	86.38	85.83	85.87
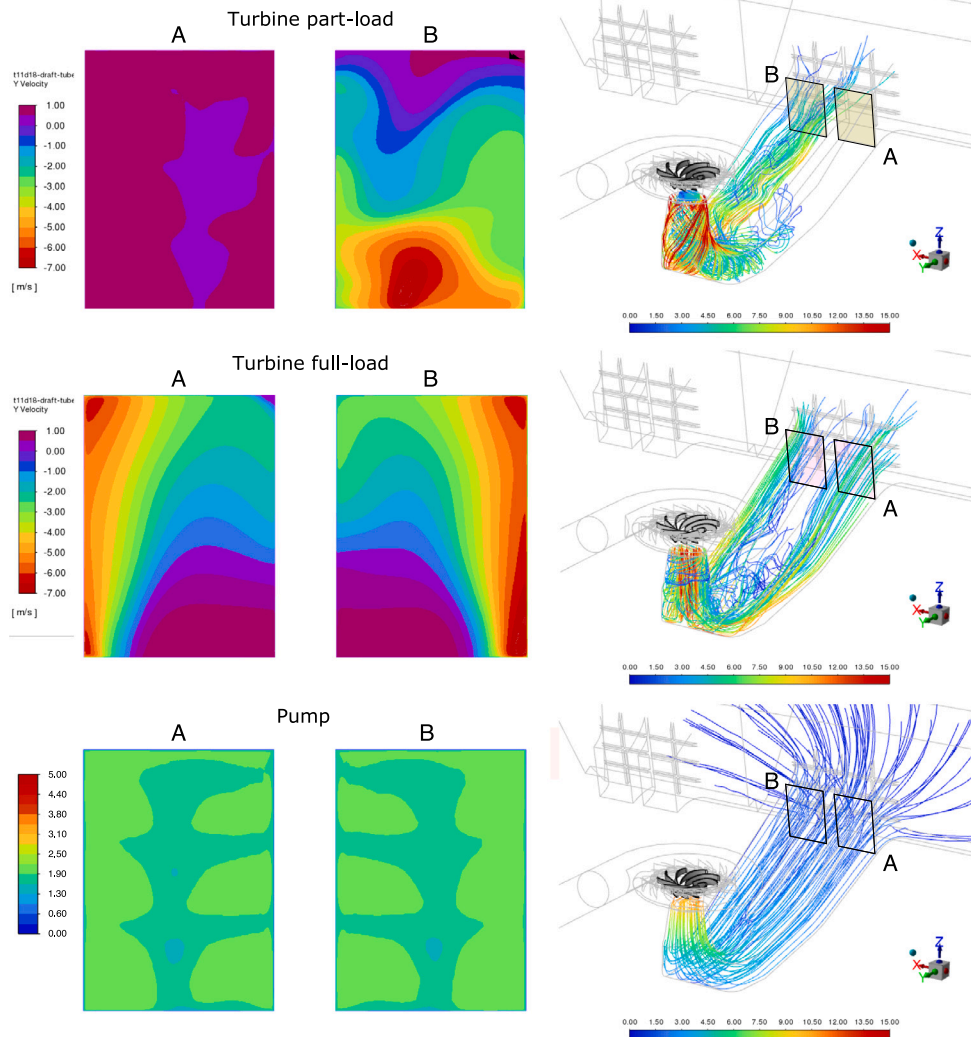
Fig. 16. Time-averaged streamlines and contours of the normal velocity component at the draft-tube exit in the turbine part load and full load and in pumping operations.

In normal pump operations, water slowly approaches the intake and the incoming streamlines are well distributed within the reservoir despite the narrowing of the available room at the bottom of the reservoir. The effect of the trash rack grid located upstream of the pump inlet section is visible and it shows to what degree it slows the flow downstream. The flow velocity magnitude is symmetrically spread in the two channels.

3.5. Pump operations

In HSC, the flow structure within the turbine draft tube only depends on the turbine operation and is not affected by the pump at its side. However, the choice of configuration where the unit is operated in turbine mode influences the pump inflow. In both HSC-operation cases (PTO, TPO) the turbine hits the angled wall in front of the draft tube and quickly exits the bottom of the reservoir. In PTO, the turbine part

load triggers large vortexes that fill the near zone on its right due to the mass flow imbalance and recirculation at the draft tube exit. Such turbulence is slow but with sufficient momentum to disturb the pump suction pipe. On the left of the turbine draft tube, the flow speed is high, and the vortex does not stall near the unit (Fig. 17).

In turbine full load operation (Fig. 18) the velocity profile is well balanced at the exit of the draft tube, and high flow speed clears the bottom of the reservoir engaging in large circulation within the whole reservoir. Such a large swirl reaches the top surface and the lateral walls of the reservoir and perturbs the inlet streamlines at the pump suction side.

The flow streamlines of the HSC - TPO, as they enter the reservoir from the turbine draft tube, resemble those of the HSC - PTO. However, the result differs due to the proximity of the lateral wall of the bottom part of the reservoir. The discharge from unit 1, when it operates in generating mode at full load, is directed primarily towards the front
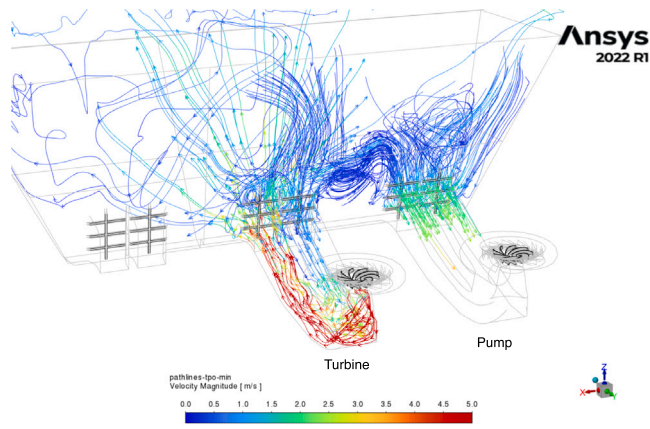
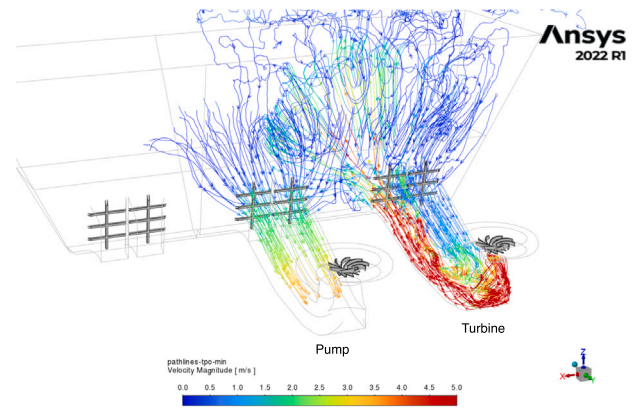**Fig. 17.** Arrowed streamlines in PTO *Pmax* operation.

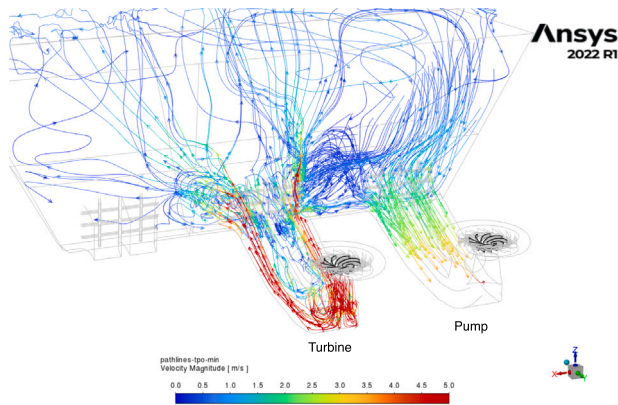**Fig. 19.** Arrowed streamlines in TPO *Pmax* operation.

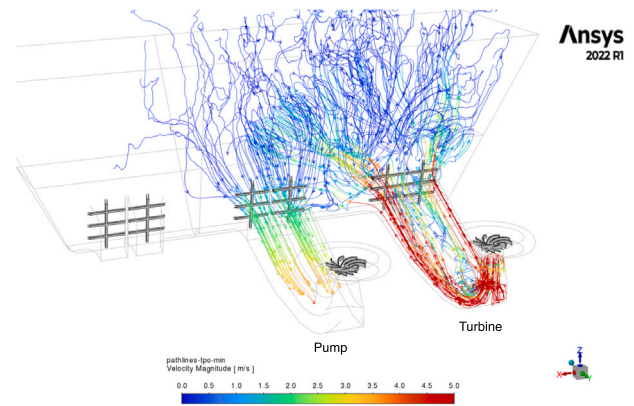**Fig. 18.** Arrowed streamlines in PTO *Pmin* operation.

Fig. 20. Arrowed streamlines in TPO *Pmin* operation.

wall and then to the second unit. This results in the creation of a substantial vortex that has ample space to develop and grow. Most importantly, when unit 2 operates in pumping mode, it effectively draws water from an undisturbed area positioned in front of unit 3, and this action does not disrupt the flow field within its intake (Fig. 20). When the turbine operates at part-load, the vortex is still not meddling at the pump intake (Fig. 19).

In both PTO and TPO operations, the velocity fields in the pump exhibit a consistent pattern of gradual acceleration as the fluid approaches the impeller. Instead, when the units are operating in turbine mode, their behavior is categorized by different operational states: in part load (HSC - *Pmax*) the draft tube has unbalanced discharge channels, while in full load both channels are engaged symmetrically. Fig. 21 illustrates the velocity magnitude at the draft-tube boundaries and midplanes, extended into the reservoir up to the front wall. Moreover, the time-averaged velocity contours at the pump entrance in HSC are shown. The flow experiences disruption at the pump inlet, leading to a slight imbalance in the discharge distribution between the two channels when compared to the baseline case, as illustrated in Fig. 16. 53.6% and 52.7% of the pump discharge pass through the first channel A for the PTO - *Pmax* and PTO - *Pmin* respectively. With the turbine operating in full load operation, the velocity profile is well balanced at the exit of the draft tube, and high flow speed clears the bottom of the reservoir engaging in large recirculation within the whole reservoir. Such a large swirl reaches the top surface and the lateral walls of the reservoir and perturbs the inlet streamlines at the pump suction side. In HSC-TPO operations, the flow appears to be not perturbed at the pump intake and a balanced discharge distribution is engaging both channels.

Eventually, having information about the flow angle at the impeller inlet is crucial for assessing if there are significant alterations in the inflow that might have adverse effects on the pump mode performance. Consequently, examining the contour of the flow angle before entering the runner is essential. The comparison is taken at the surface next to the impeller suction side, as shown in Fig. 22. The velocity angle is a function of the tangential-to-axial velocity ratio as defined in $\alpha = atan(v_t/v_a)$ and it indicates the inherent rotation of flow entering the pump. For efficient pump performance, it is desirable to keep the magnitude of these values relatively low, and preferably within ±7° [17]. When looking from above, positive values indicate a swirl in an anticlockwise direction, conversely negative values indicate a swirl in a clockwise direction. Swirl predictions for the impeller inlet at HCS-TPO illustrate an unaffected pattern for the velocity angle. However, in PTO the velocity angle evolves into another shape and it lays within the same limits as in OPO, namely ±9.7°. It is also relevant to notice the swirl pattern is off-centred but with a loose symmetry. On the other hand, the axial velocity comparison does not depict a significant difference in discharge distribution that would indicate a risk for the operation in HSC. All the profiles linger around 10 m/s of axial velocity, with a lower velocity central point due to the close presence of the impeller nose.

Because of the velocity angle distortion at the impeller leading edge, unforeseen cavitation phenomena might occur in pumping. Fig. 23 illustrates the static pressure on a parallel xy-plane near the impeller inlet, sectioning the nose of the hub. Moreover, a relative static pressure iso-surface at 0 Pa is created to help define the instantaneous profile of the pressure field by the nine blades. Iso-surfaces of the pressure of incipient cavitation are shown as well. The region where pressure is lower than the vapour pressure extends marginally at the pressure side
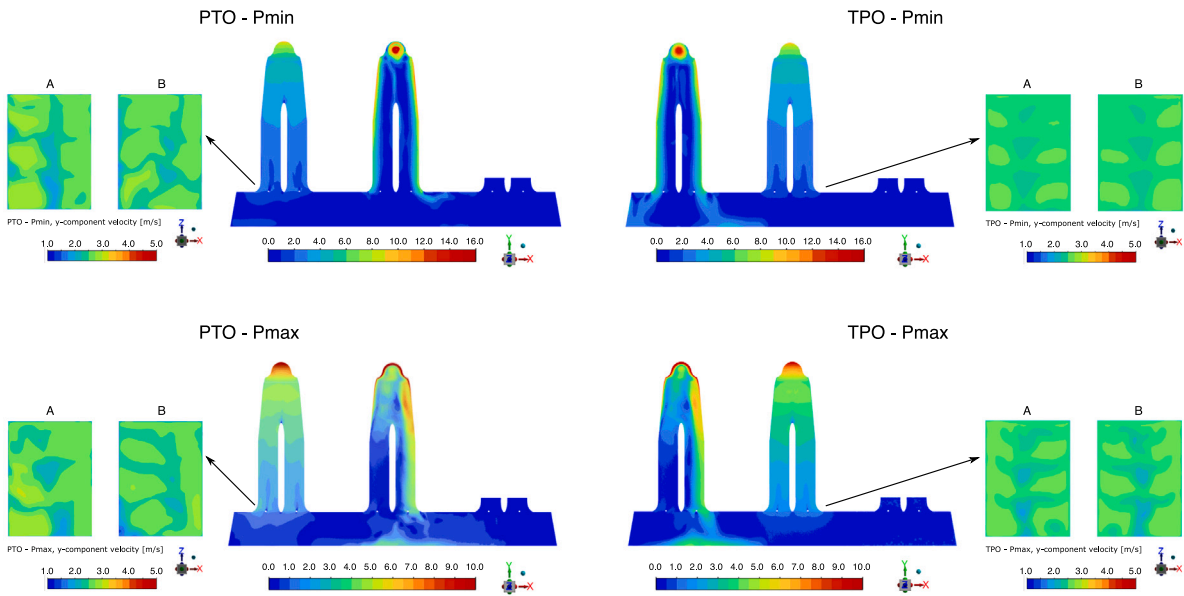
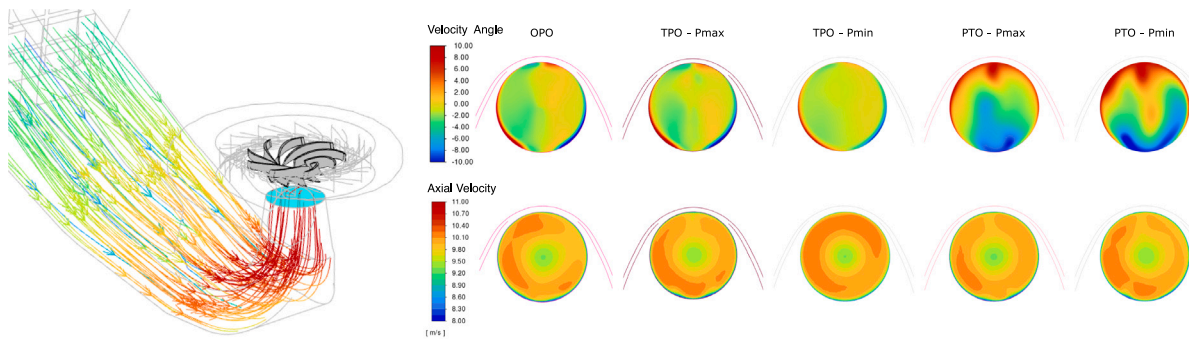**Fig. 21.** Time-averaged (0.36) velocity magnitude contours at the draft-tube boundaries and midlanes.

Fig. 22. Comparison of the velocity angle contours and axial profile between pump mode (OPO) and HSC operations.
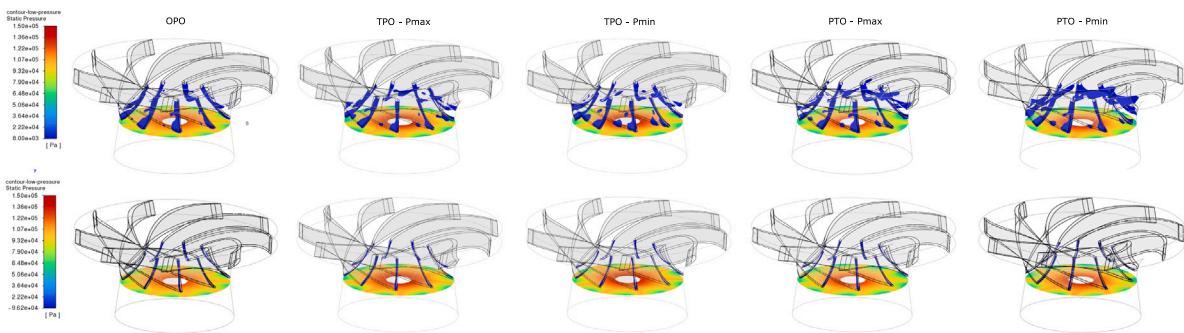

Fig. 23. Static pressure field comparison in HSC and pump mode. Top: iso-surfaces at 0 Pa relative pressure; bottom: iso-surfaces at incipient cavitation −96 kPa relative pressure.

of the leading edge also in all the cases, the baseline case included. A 48 kPa hydrostatic pressure increase would be sufficient to phase out possible harmful conditions. The baseline case OPO exhibits an identical pressure pattern at the impeller inlet and analogous surface dimensions for the incipient cavitation characteristic. Hence, tested HSC operations do not result in more adverse effects than those experienced during normal pumping mode.

For a comprehensive analysis of the velocity angle disturbance, plots of the pressure along three streamlines are presented in Fig. 24. Here, one can compare the blade loading at 20%, 50%, and 80% spans with the OPO case. The continuous line represents averaged values over the impeller's nine blades and the shaded area is within the standard deviation. Besides the expected peaks at leading and trailing edges, the progressive increase of pressure along the pressure side and suction side is confirmed to be regular. There are no shocks, negative incidences, or
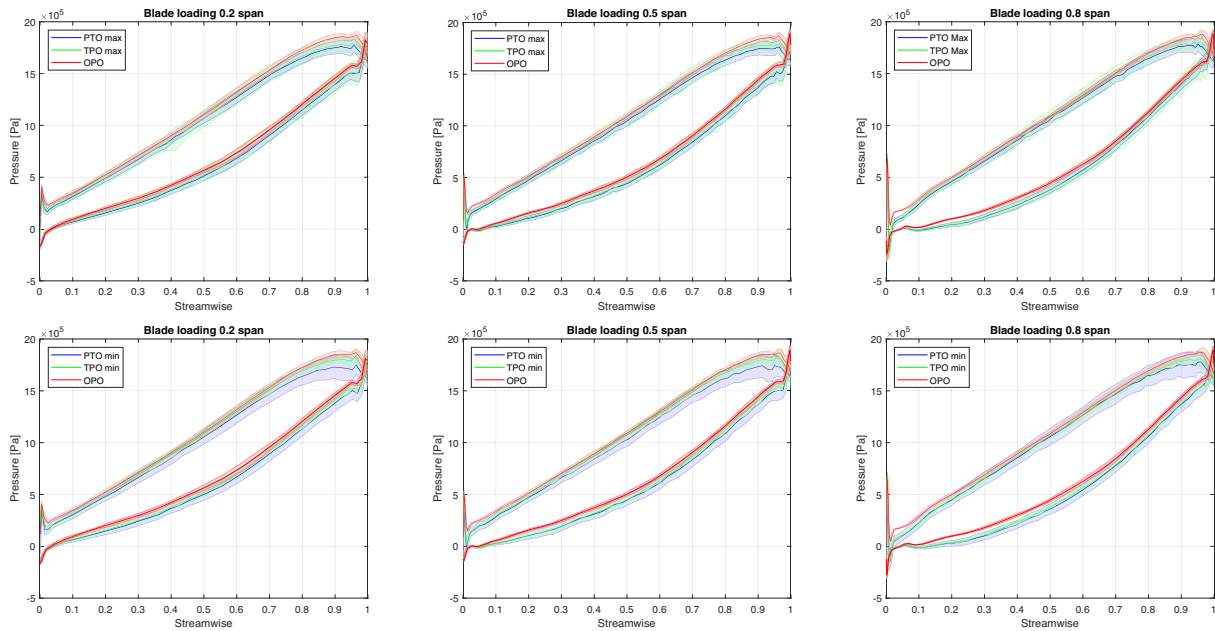
Fig. 24. Pump blade loading comparisons of pumping mode and HSC operations at 20%, 50%, and 80% spans.
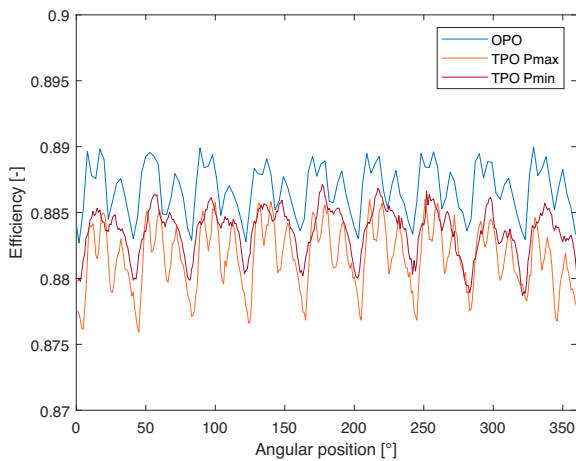

Fig. 25. Efficiency comparison plot for OPO and HSC - PTO.

pressure dips observed during the HSC operations. Nevertheless, while the TPO accurately mirrors the trend of the blade loading in pumping mode, the PTO registers a lower delivered head. In this matter, the pump efficiencies during PTO operations are compared as well Fig. 25. The plot of the pump efficiency is recorded within a complete impeller rotation in PTO configurations. The HSC outputs have been gathered by simulations with the resolution of 1°-degree rotation per time-step (namely $4.444 \cdot 10^{-4}$ s). It is evident that they are lower than the baseline but they remain consistent regardless of the specific turbine operation in HSC (part or full load). The time-averaged values of the efficiency reported in the last full period are 88.17% and 88.36% for PTO - *Pmax* and PTO - *Pmin* respectively. OPO operation reaches 88.68% average.

3.6. Air entrainment risk

The presence of vortices within the reservoir can lead to the entrainment of air or gas in the pump intakes, even if the unit is fully submerged. In severe instances of free surface vortex reaching the pump intake, the air entrainment can result in unpredictable or noisy pump

operation, as well as a decrease in overall pump performance. Entrained air can accumulate in the pump and, in extreme cases, obstruct the impeller eye, leading to a loss of torque. Air entrainment is difficult to capture with CFD analysis, especially when free surface effects are important. To assess the potential risk of air entrainment in the pump-turbine runner, conducting multiphase modeling is considered the most effective approach [18]. These simulations can predict the presence or absence of air within the runner at the expense of large computational resources [19,20]. However, when utilizing single-phase simulations, other acceptance criteria need to be considered [18,21]. Identifying the formation of dye cores at the intake [17] is explained by using a single-phase model imposing frictionless free-slip wall of the water surface boundary condition. The velocity approaches zero near the no-slip boundary but increases gradually to a free stream, relatively constant velocity before reducing again at water-air surface [20]. This depth-independent characteristic of the flow velocity away from the boundaries approximately agrees with the free slip condition. Under these conditions and with the reference pressure set at the top of the tailwater (which is 17.7 meters above the pump intake), it is possible to detect the water depression by monitoring the pressure variation on the free surface. This enables the quantification of local areas of depression (or surface dimples or vortexes) (Fig. 26). Subtracting the hydrostatic pressure (oriented in *z*-direction), multiple surfaces are generated only to offer more insights into the submerged currents phenomena.

In OPO no depression is exhibited other than a light numerical effect of the flow incoming from the side of the river. In the PTO – *Pmax* case, a submerged vortex generated by the turbine as described in Fig. 17 pushes the pump suction cone aside against the lateral wall, narrowing the available drawable volume. A weak depression area is indeed traceable on the free surface. In PTO – *Pmin* case, no sign of water level depression is reported at the free surface. Beneath it, the effect of a large recirculation in the bottom reservoir is visible in areas of low pressure.

4. Discussion: PSPP dispatch adjustment in HSC

The presented numerical methodology and the results of the 3D numerical simulations prove that PSPP operational set-points in HSC differ from the normal service. As part of the discharge crosses the
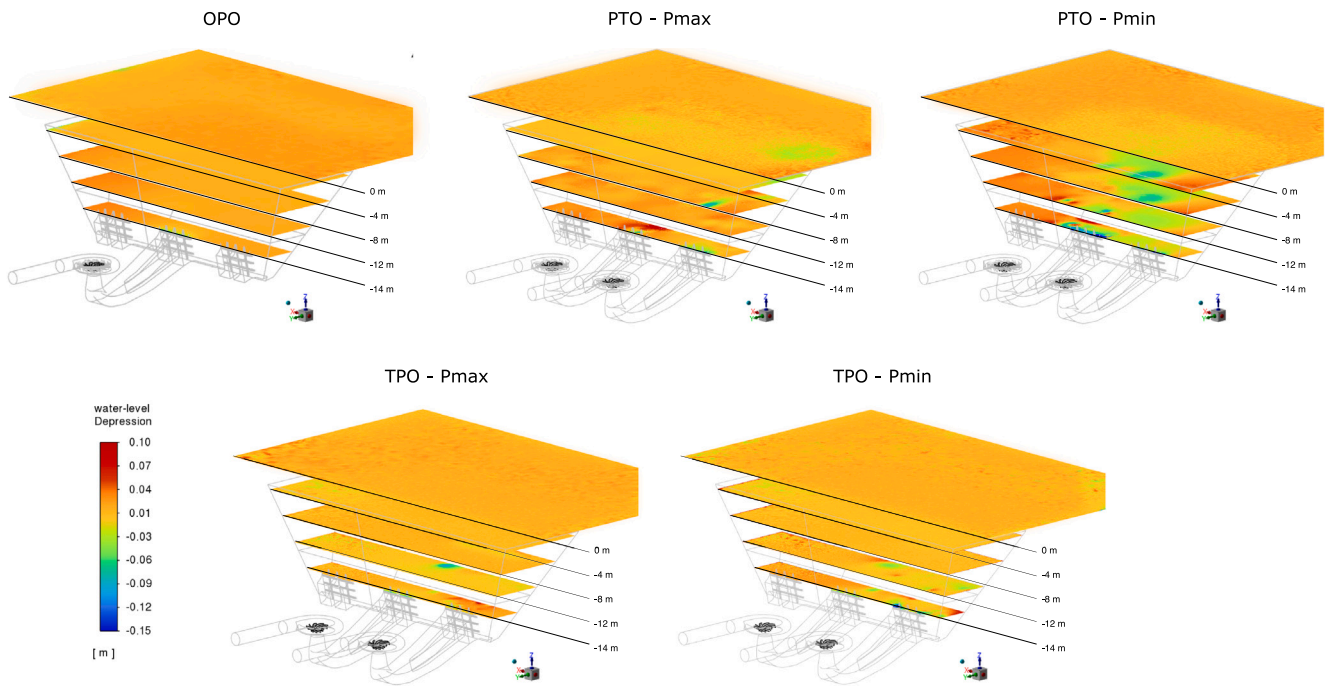
Fig. 26. Representation of water level depression at free-slip wall river and illustrations of submerged other levels.

water circuit towards the turbine and part is pumped to the upper reservoir, the system characteristics need to comply with the combined losses of the two parallel branches. Therefore the available head delivered by the pump changes. The results of the CFD analysis shed light on the operational range limits of the pump and turbine concerning the admissible boundaries for continuous operation. The redesigned control system for HSC operations must prioritize dispatching based on the results of this investigation, including the predicted pressure losses in the trifurcation (Fig. 9). Above all, it is evident that specific configurations are more favorable in terms of pressure losses between the pumping and generating units. The average head loss between the units is approximately 2 m, with the most unfavorable scenario occurring during PTP - *Pmin* operation, where it reaches nearly 4 m. Additionally, it is crucial to prioritize the safe operation of the units and maintain high efficiency. Besides CFD analysis proving safe operations are being met, a different set-point than normal turbine operations is needed to match the rated power output. Indeed, the residual swirl of the flow exiting the trifurcation may result in increased losses within the turbine casing, leading up to an efficiency reduction of 0.51–0.55% respectively in the PTO - *Pmax* and POT - *Pmax*, bringing consequent power alterations if guide vanes are not properly adjusted.

Regarding the conditions downstream of the trifurcation, the graphics demonstrate that there is a low velocity within the gap of the reservoir between the two units (≤ 1 m/s), testing no severe interactions. The performance of the turbine in HSC mode remains similar to its normal functioning. However, the off-centre swirl that the pump needs to endure in TPO delivers a velocity angle deviation a few degrees higher than the recommended best practice leading to a reduction in efficiency ranging from 0.3% to 0.5%. For this matter, the HSC-TPO configuration is endorsed over the PTO.

Furthermore, the minimum admissible water level of the lower reservoir ensures its correlation and consistency with the most problematic situation of the pump units. In all the tested configurations, low pressure at the impeller inlet is expected, and it is reported the possibility of attached cavitation or leading-edge cavitation. An additional increase in the water level limit (≥ 5 m) of the lower reservoir is then recommended for pumping and HSC operations. Eventually, no alarming instances of air entertainment are recorded.

Although the comprehensive performed CFD analysis on HSC implementation, this mode requires performing compelling inspections and additional investigations are due before initializing HSC operations and will be the subject of future work. To fully ensure the safe operation of the power plant during HSC a transient analysis of the whole hydraulics and electrical system has to be performed. With 1D simulations, the most critical load cases in HSC operation can be described to identify the potential hydraulic transient issues [22] and in particular conditions as in an emergency shutdown transient process [23]. Ultimately, the acquisition of on-site data through measurements of pressure pulsations and vibrations in strategically sensitive zones proximate to the trifurcation, or the quantification of losses within specified regions, will establish a substantiated technical framework [5].

To extend the outcomes of this research to broader perspectives, here are five key objectives to consider when assessing HSC implementation in any suitable PSPP:

1. Operational Set-Points Adjustment: The numerical analysis reveals that operational set-points for PSPP during HSC operations differ from normal service. Thus, adjusting set-points to optimize performance in HSC mode is needed.

2. System Characteristics Compliance: The system must account for combined losses in the water circuit, considering both the flow to the turbine and that pumped to the upper reservoir. Ensuring that the system characteristics align with these losses is crucial for maintaining operational efficiency.

3. Operational Range Limits Identification: Understanding the operational characteristics in discharge, tailwater head and lower reservoir topography aid in narrowing down the scenarios to investigate for PSPPs during HSC mode. Relying solely on the cases per maximum and minimum PSPP power consumption in HSC mode in the analysis seems adequate for detecting the potential operational issues and limits of the units during continuous operations.

4. Redesigned Control System Priority: A redesigned control system for HSC operations should prioritize dispatching based on investigation results, particularly considering predicted pressure

losses in the trifurcation and hydraulic efficiency detriments endorsing a favorable configuration over others. This prioritization ensures efficient and safe operation of the PSPP.

5. Safety and Efficiency Maintenance Strategy: While implementing HSC mode, maintaining safe operation and high efficiency is paramount. Ensuring that units operate within safe parameters and to minimize efficiency reduction due to running units interaction is essential for optimal performance.

5. Conclusions

This work presents a validated 3D numerical model to investigate the HSC feasibility in a PSPP that has not been intended for such applications addressing the possible complications of this operation. The computation of the flow structure in the trifurcation presents the correlation of total pressure losses and the flow patterns per each HSC operation; it also proves the adverted danger of fluid pulsations or cavitation. Additional analysis is performed to verify the safe operations of the turbine under the resulting velocity profiles entering the turbine spiral casing. No fluid-dynamic hazardous operations are met with the incoming flow pattern coming from the trifurcation in HSC operations. Still, possible efficiency detriments can occur due to the additional friction losses.

The analysis of the domain downstream of the trifurcation, specifically the interaction of units in HSC connected by the shared reservoir, reveals fluid dynamic conditions that are similar to the pre-existing operating conditions in turbine mode. Moreover, these conditions are not found to pose any additional risks to the pump operations, albeit there is a possibility of a reduction in hydraulic efficiency. Encouragingly, the analysis conducted through CFD indicates that there is no presence of dye core near the intake, and harmful vortices are not reaching the pump eye. This suggests that air entrainment from the free surface does not cause any adverse effects on the pump operation.

Finally, the analysis performed on the existing PSPP constitutes a decisive contribution to the comprehensive feasibility assessment of implementing HSC operations and in identifying the optimal operation. The illustrated observations lead to the application of additional criteria for the governing control of the PSPP in HSC. The outcomes of this paper play a vital role in defining the criteria for choosing the most suitable HSC configuration and promoting the flexibility gain that such operations can provide to hydroelectric power plants while maintaining safety. The developed methodology can be replicate on any PSPP for an extensive evaluation of HSC feasibility at global scale.

CRediT authorship contribution statement

Alessandro Morabito: Writing – review & editing, Writing – original draft, Methodology, Investigation, Formal analysis, Data curation, Conceptualization. **Elena Vagnoni:** Writing – review & editing, Supervision, Methodology, Funding acquisition, Conceptualization.

Declaration of competing interest

The authors declare that they have no known competing financial interests or personal relationships that could have appeared to influence the work reported in this paper.

Data availability

The authors do not have permission to share data.

Acknowledgments

Appendix

See Table 6.

Table 6
Additional info of the CFD validation of the prototype unit in turbine and pump mode.

Turbine mode								
discharge	GVO	turbine head	runner head	torque	power	n11	Q11	efficiency
$Q/Q_{n,t}$	[°]	$H/H_{n,t}$	$H/H_{n,t}$	[M N m]	$P/P_{n,t}$	[rpm]	[m³/s]	[%]
1.00	24.6	1.084	1.059	2.01	1.10	44.407	0.623	93.70
1.00	25.6	1.030	1.004	1.91	1.04	45.568	0.639	93.92
1.00	26.1	1.001	0.978	1.84	1.01	46.215	0.648	93.17
1.00	26.6	0.976	0.956	1.79	0.98	46.808	0.657	92.71
1.00	27.6	0.941	0.920	1.69	0.92	47.668	0.669	90.88
1.00	28.6	0.900	0.880	1.60	0.87	48.727	0.684	89.98
1.00	29.6	0.877	0.847	1.51	0.82	49.365	0.692	87.13
1.00	31.6	0.813	0.789	1.38	0.75	51.297	0.720	86.05
1.00	35.6	0.724	0.704	1.16	0.63	54.338	0.762	81.07
1.02	26.1	1.033	1.008	1.94	1.06	45.489	0.653	93.38
0.98	26.1	0.970	0.949	1.73	0.94	46.952	0.643	92.53
0.95	26.1	0.943	0.925	1.63	0.89	47.605	0.637	91.94
0.93	26.1	0.917	0.902	1.53	0.84	48.296	0.630	91.13
0.91	26.1	0.893	0.880	1.44	0.79	48.945	0.623	90.04

Pump mode								
discharge	GVO	pump head	impeller head	torque	power	n11	Q11	efficiency
$Q/Q_{n,p}$	[°]	$H/H_{n,p}$	$H/H_{n,p}$	[M N m]	$P/P_{n,p}$	[rpm]	[m³/s]	[%]
1.00	24.6	1.014	1.104	2.02	1.04	−45.664	−0.566	88.56
1.00	26	1.003	1.102	2.01	1.03	−45.931	−0.569	88.01
1.00	28	1.019	1.111	2.07	1.07	−45.555	−0.565	86.81
1.00	30	1.013	1.117	2.07	1.07	−45.686	−0.566	86.24
0.85	24.6	1.098	1.162	1.89	0.97	−43.887	−0.465	87.67
1.09	24.6	0.969	1.034	2.08	1.07	−46.704	−0.633	89.63
1.09	25	0.966	1.032	2.07	1.07	−46.787	−0.635	89.74

References

[1] International Energy Agency. Renewable information 2021: database documentation. 2021, https://www.iea.org.

[2] Smith BT, Zhang QF, Cones M, Anders J. HAP best practice catalog revision 2.0. Tech. rep, Oak Ridge, TN (United States): Oak Ridge National Lab.(ORNL); 2022.

[3] Chazarra M, Pérez-Díaz JI, García-González J. Optimal energy and reserve scheduling of pumped-storage power plants considering hydraulic short-circuit operation. IEEE Trans Power Syst 2017;32:344–53.

[4] Iliev I, Trivedi C, Dahlhaug OG. Variable-speed operation of francis turbines: A review of the perspectives and challenges. Renew Sustain Energy Rev 2019;103:109–21.

[5] Gaal T, Sallaberger M. Pumped storage machines–hydraulic short-circuit operation. Adv Energy Storage: Latest Develop R&D Mark 2022;289–301.

[6] Kwon J, Levin T, Koritarov V. Optimal market participation of pumped storage hydropower plants considering hydraulic short-circuit operation. In: 2020 52nd North American power symposium. IEEE; 2021, p. 1–6.

[7] Chazarra M, Pérez-Díaz JI, García-González J. Economic viability of pumped-storage power plants equipped with ternary units and considering hydraulic short-circuit operation. J Phys Conf Series 2017;813:012013.

[8] Landry C, Nicolet C, Badina C, Pichon H, Drommi J. Contribution for the roadmap of hydraulic short circuit implementation: Case of grand-maison pumped storage power plant. In: IOP conference series: earth and environmental science, vol. 1079, no. 1. IOP Publishing; 2022, 012107.

[9] Alharbi H, Bhattacharya K. Participation of pumped hydro storage in energy and performance-based regulation markets. IEEE Trans Power Syst 2020;35(6):4307–23.

[10] Nicolet C, Pannatier Y, Kawkabani B, Schwery A, Avellan F, Simond J. Benefits of variable speed pumped storage units in mixed islanded power network during transient operation. Proc HYDRO 2009;26–8.

[11] Pérez-Díaz JI, Sarasúa JI, Wilhelmi JR. Contribution of a hydraulic short-circuit pumped-storage power plant to the load–frequency regulation of an isolated power system. Int J Electr Power Energy Syst 2014;62:199–211.

[12] Huber B, Korger H, Fuchs K. Hydraulic optimization of a T-junction hydraulic model tests and CFD-simulation. In: Proc. XXXI iAHR congress, seoul, Korea. 2005.

[13] Decaix J, Drommi J-L, Avellan F, Münch-Alligné C. CFD simulations of hydraulic short-circuits in junctions, application to the grand'maison power plant. IOP Conf Series: Earth Environ Sci 2022.

[14] Morabito A, Wu C, Sigali S, Vagnoni E. CFD simulation for hydraulic short-circuit feasibility analysis. In: Proceeding ViennaHydro, 09-11 November, Vienna - Austria | 21st international seminar on hydropower plants. 2022.

[15] Tiwari G, Kumar J, Prasad V, Patel VK. Utility of CFD in the design and performance analysis of hydraulic turbines—A review. Energy Rep 2020;6:2410–29.

[16] IEC. Hydraulic Turbines, Storage Pumps and Pump- Turbines-Model Acceptance Tests. In: IEC 60193 Standard - international electrotechnical commission Geneva. Nov. 1999, p. 578.

[17] American National Standard for Pump Intake Design. ANSI/HI 9.8-1998. Tech. rep, Hydraulic Institute Standards; 2009.

[18] Ahn S-H, Xiao Y, Wang Z, Zhou X, Luo Y. Numerical prediction on the effect of free surface vortex on intake flow characteristics for tidal power station. Renew Energy 2017;101:617–28.

[19] Shukla SN, Kshirsagar JT, et al. Numerical prediction on air entrainment in pump intakes.. In: Proceedings of the 24th international pump users symposium. Texas A&M University. Turbomachinery Laboratories; 2008.

[20] Zhang J, Yee T. Extent, capacity and possibilities of computational fluid dynamics as a design tool for pump intakes: a review. Water Sci Technol Water Supply 2018;18(5):1518–30.

[21] Škerlavaj A, Škerget L, Ravnik J, Lipej A. Predicting free-surface vortices with single-phase simulations. Eng Appl Comput Fluid Mech 2014;8(2):193–210.

[22] Landry C, Nicolet C, Badina C, Pichon H, Drommi J. Contribution for the roadmap of hydraulic short circuit implementation: Case of grand-maison pumped storage power plant. In: IOP conference series: earth and environmental science, vol. 1079. IOP Publishing; 2022, 012107.

[23] Geiger C, Riedelbauch S. Power plant transients including hydraulic short circuit operation mode. Energies 2023;16(11).